Mechanisms of Reduced Striatal NMDA Excitotoxicity in Type I Nitric Oxide Synthase Knock-Out Mice

Cenk Ayata,[1] Gamze Ayata,[1] Hideaki Hara,[1] Russel T. Matthews,[2] M. Flint Beal,[2] Robert J. Ferrante,[5,6] Matthias Endres,[1] Albert Kim,[1] Richard H. Christie,[3] Christian Waeber,[1] Paul L. Huang,[4] Bradley T. Hyman,[3] and Michael A. Moskowitz,[1]

[1]Stroke and Neurovascular Regulation Laboratory, [2]Neurochemistry Laboratory, [3]Alzheimer's Disease Research Unit, and [4]Cardiovascular Research Center, Departments of Medicine, Neurosurgery, and Neurology, Massachusetts General Hospital, Harvard Medical School, Charlestown, Massachusetts, 02129, [5]Geriatric Research and Extended Care Center Unit, Bedford Veterans Affairs Medical Center, Bedford, Massachusetts 01730, and [6]Departments of Neurology and Pathology, Boston University School of Medicine, Boston, Massachusetts, 02118

We investigated the role of neuronal (type I) nitric oxide synthase (nNOS) in NMDA-mediated excitotoxicity in wild-type (SV129 and C57BL/6J) and type I NOS knock-out ($nNOS^{-/-}$) mice and examined its relationship to apoptosis. Excitotoxic lesions were produced by intrastriatal stereotactic NMDA microinjections (10–20 nmol). Lesion size was dose- and time-dependent, completely blocked by MK-801 pretreatment, and smaller in nNOS knock-out mice compared with wild-type littermates ($nNOS^{+/+}$, 11.7 ± 1.7 mm^3; $n = 8$; $nNOS^{-/-}$, 6.4 ± 1.8 mm^3; $n = 7$). The density and distribution of striatal NMDA binding sites, determined by NMDA receptor autoradiography, did not differ between strains. Pharmacological inhibition of nNOS by 7-nitroindazole (50 mg/kg, i.p.) decreased NMDA lesion size by 32% in wild-type mice ($n = 7$). Neurochemical and immunohistochemical measurements of brain nitrotyrosine, a product of peroxynitrite formation, were increased markedly in wild-type but not in the $nNOS^{-/-}$ mice. Moreover, elevations in 2,3- and 2,5-dihydroxybenzoic acid levels were significantly reduced in the mutant striatum, as a measure of hydroxyl radical production.

The importance of apoptosis to NMDA receptor-mediated toxicity was evaluated by DNA laddering and by quantitative histochemistry [terminal deoxynucleotidyl transferase-mediated deoxyuridine triphosphate–biotin nick end-labeling (TUNEL) staining]. DNA laddering was first detected within lesioned tissue after 12–24 hr. TUNEL-positive cells were first observed at 12 hr, increased in number at 48 hr and 7 d, and were located predominantly in proximity to the lesion border. The density was significantly lower in $nNOS^{-/-}$ mice. Hence, oligonucleosomal DNA breakdown suggesting apoptosis develops as a late consequence of NMDA microinjection and is reduced in nNOS mutants. The mechanism of protection in $nNOS^{-/-}$ mice may relate to decreased oxygen free radical production and related NO reaction products and, in part, involves mechanisms of neuronal death associated with the delayed appearance of apoptosis.

Key words: NMDA; excitotoxicity; striatum; neuronal nitric oxide synthase; knock-out mice; nitrotyrosine; hydroxyl radical; apoptosis; DNA laddering; TUNEL staining

Nitric oxide ($NO^{\bullet}$) synthesized by neuronal (type I) nitric oxide synthase (nNOS) has been implicated in many pathophysiological processes, including cerebral ischemia and excitotoxicity (Bredt and Snyder, 1990; Dawson et al., 1991; Lipton et al., 1993; Moskowitz and Dalkara, 1996). A number of studies have demonstrated that pharmacological inhibition or gene knock-out of nNOS confers resistance to cerebral ischemia (Dalkara et al., 1994; Huang et al., 1994) and excitotoxicity *in vivo* and *in vitro* (Dawson et al., 1996). In particular, cortical cells in culture from $nNOS^{-/-}$ mice are resistant to NMDA but not AMPA or kainic acid (KA) receptor-mediated toxicity (Dawson et al., 1996). Pharmacological inhibition of type I NOS protects against intrastriatal NMDA- but not AMPA- or KA-induced excitotoxic lesions (Schulz et al., 1995). Contradictory results have been reported about the importance of nNOS to excitotoxicity (for review, see Pelligrino, 1993; Löschmann et al., 1995), part of which may be explained by the deleterious effects of endothelial (type III) NOS (eNOS) inhibition (Morikawa et al., 1992; Connop et al., 1995; Globus et al., 1995; Huang et al., 1996) and/or insufficient type I NOS inhibition.

Two mechanistically distinct but related forms of neuronal death have been identified and take the form of necrosis or apoptosis. Both $NO^{\bullet}$ and peroxynitrite have been linked to apoptosis in several *in vitro* models (Albina et al., 1993; Estevez et al., 1995; Lin et al., 1995). Oxidative DNA damage and strand breaks caused by peroxynitrite are well documented (Inoue and Kawanishi, 1995; Salgo et al., 1995), which might suggest a mechanism for initiating apoptosis after NMDA receptor activation and $NO^{\bullet}$ synthesis. Because decreased neuronal NOS activity is neuroprotective in stroke and excitotoxicity, and because blockade of apoptosis de-

Received May 23, 1997; revised June 25, 1997; accepted July 7, 1997.

This work was supported by the Massachusetts General Hospital Interdepartmental Stroke Program Project NS10828 (M.A.M.), an unrestricted award in neuroscience by Bristol-Myers Squibb (M.A.M.), the Huntington's Disease Society of America (R.J.F.), the Department of Veterans Affairs (R.J.F.), National Institutes of Health Grants AG12922 (R.J.F. and M.F.B.), 1P30AG13846 (R.J.F.), NS35255 (R.J.F.), NS33335 (P.L.H.), and AG08487 (B.T.H.), and Deutsche Forschungsgemeinschaft Grant En 343/1-1 (M.E.). P.L.H. is an Established Investigator of the American Heart Association. We thank Karen Smith and Tom Kilgallen for their technical assistance.

Correspondence should be addressed to Michael A. Moskowitz, Stroke and Neurovascular Regulation Laboratory, CNY 149-6403, 13th Street, Charlestown, MA 02129.

Copyright © 1997 Society for Neuroscience 0270-6474/97/176908-10$05.00/0

creases cell death and improves functional recovery (Hara et al., 1997a), it is therapeutically relevant to investigate mechanisms of cell death induced by nitric oxide and its reaction products.

Mice with a disruption of the type I NOS gene provide an invaluable tool to study the physiological and pathophysiological functions of NO• (P. L. Huang et al., 1993; Z. Huang et al., 1994; Hara et al., 1996; Ma et al., 1996; Panahian et al., 1996). In this study, we demonstrate that intrastriatal microinjection of NMDA leads to neuronal death, that the absence of NO• synthesized by type I NOS affords 50% protection, and that apoptosis is involved as a late event. The neuroprotection attained in $nNOS^{-/-}$ mice probably relates to a decreased production of OH• radicals and reduced nitration of tyrosine by elimination of the NO• and $O_2^{\bullet -}$ reaction and subsequent peroxynitrite formation. Our data also suggest that apoptosis is an important delayed mechanism for NO•-mediated excitotoxicity after NMDA receptor activation.

MATERIALS AND METHODS

Experimental animals

Wild-type (SV129 and C57BL/6J, 21–27 gm, male; Taconic Farms, Germantown, NY) and type I NOS knock-out mice (20–28 gm, male and female) were housed under diurnal lighting conditions and given food and water *ad libitum*. In preliminary experiments we observed a significantly larger NMDA (10 and 20 nmol) lesion in SV129 mice compared with C57BL/6J mice; therefore, comparison of the lesion volume, DNA laddering, and terminal deoxynucleotidyl transferase (TdT)-mediated deoxyuridine triphosphate (dUTP)–biotin nick end-labeling (TUNEL)-positive cells were performed in littermate wild-type offspring from the mating of heterozygotes ($nNOS^{+/-}$) as controls to eliminate differences attributable to background strains.

Intrastriatal NMDA microinjection

Mice were anesthetized with halothane (2.5% for induction, 1–1.5% for maintenance), and body temperature was kept at 36.9 ± 0.1°C with a thermostatic heating pad. The head was fixed to a stereotaxic frame with a mouse head holder (David Kopf, Tujunga, CA). A burr hole was drilled, and an injection needle (26 ga) was lowered into the right striatum (anterior, 0.5 mm; lateral, 2.5 mm; ventral, 2.5 mm, from bregma). Drugs were injected in a volume of 0.3 μl, over 2 min, using a microinjection system (David Kopf), and the needle was left in place for an additional 8 min.

Mice were routinely killed by decapitation after brief halothane anesthesia, at 48 hr. To study lesion development, mice were killed at 3, 6, 12, 24, and 48 hr and 7 d after injection. The brains were frozen, and 20-μm-thick coronal cryostat sections were taken. Every 10th section was stained by hematoxylin and eosin (H&E). The lesion area was identified by the loss of basophilic staining, measured by image analysis (M4, Imaging Research, St. Catharines, Ontario, Canada), and integrated to calculate the volume.

Drug preparation

NMDA was dissolved in 0.1 M PBS, pH 7.4, at 33 and 67 mM. 7-nitroindazole (7-NI) was dissolved in peanut oil (5 mg/cc), administered 30 min before intrastriatal NMDA microinjection (25 mg/kg, i.p.), and repeated 30 min later. MK-801 (4 mg/kg, i.p., in normal saline) was administered 30 min before intrastriatal NMDA microinjection.

Salicylate assay and 3-nitrotyrosine measurement

The salicylate hydroxyl-trapping method (Floyd et al., 1984) was used for measuring OH• radicals in striatal tissues 1, 6, and 24 hr after intrastriatal injection of NMDA (20 nmol). Salicylate (100 mg/kg, i.p.) was administered 1 hr before killing. Mice were killed by decapitation, and the right and left striata were rapidly dissected from a 2-mm-thick slice on a chilled glass plate, and the tissues were placed in 0.5 ml of chilled 0.1 M $HClO_4$. The samples were sonicated, frozen rapidly, thawed, and centrifuged twice. Aliquots of the supernatant were stored at −70°C until assay. Salicylate and its metabolites 2,3- and 2,5-dihydroxybenzoic acid (DHBA) were quantified by HPLC with 16-electrode electrochemical detection. Salicylate, 2,3- and 2,5-DHBA, tyrosine, and 3-nitrotyrosine were measured electrochemically by oxidation at 840, 240, 120, 600, and 840 mV, respectively, with retention times of 20.5, 9.4, 6.3, 10.5, and 18.2 min, respectively. The 3-nitrotyrosine measurements were validated by changing chromatographic conditions, overspiking samples with authentic standards, and demonstrating the correct electrochemical signature across two electrodes. Treatment of both standards and tissue extracts with 1 M sodium hydrosulfite (dithionite) abolished the 840 mV nitrotyrosine peaks by conversion of 3-nitrotyrosine to aminotyrosine. Data were expressed as the ratio of 2,3- and 2,5-DHBA to salicylate and of 3-nitrotyrosine to tyrosine to normalize for varying brain concentrations of salicylate and tyrosine, which could be a consequence of impairment of blood–brain barrier (salicylate), or neuronal loss during treatment (tyrosine).

Nitrotyrosine immunohistochemistry

$nNOS^{-/-}$ ($n = 2$) and wild-type (SV129, $n = 5$) mice were processed for immunohistopathological examination. Mice were deeply anesthetized and transcardially perfused with cold (4°C) saline, followed by 0.1 M sodium phosphate buffer, pH 7.4, paraformaldehyde solution. Brains were removed directly after perfusion, post-fixed for 2 hr, washed in 0.1 M sodium phosphate buffer, and cryoprotected in increasing concentrations of 10 and 20% glycerol-2% DMSO solution. Frozen serial coronal sections of the entire brain were made at 50 μm intervals. Sections were subsequently stained for Nissl substance using cresyl violet to identify the lesioned locus and for immunohistochemical localization of 3-nitrotyrosine (monoclonal antibody marker for peroxynitrite-mediated nitration; Upstate Biotechnology, Lake Placid, NY; 1:500 dilution) using a previously reported conjugated second antibody method (Ferrante et al., 1993). Tissue sections were preincubated in absolute methanol-0.3% hydrogen peroxide solution for 30 min, washed (three times) in PBS, pH 7.4, 10 min each, placed in 10% normal goat serum (Life Technologies, Gaithersburg, MD) for 1 hr, incubated free floating in primary antiserum at room temperature for 12–18 hr (all dilutions of primary antisera above included 0.3% Triton X-100 and 10% normal goat serum), washed (three times) in PBS for 10 min each, placed in peroxidase-conjugated goat anti-rabbit IgG (1:300 in PBS; Boehringer Mannheim, Mannheim, Germany), washed (three times) in PBS 10 min each, and reacted with 3,3′-diaminobenzidine-HCl (1 mg/ml) in Tris·HCl buffer with 0.005% hydrogen peroxide.

Specificity for the antisera used in this study was examined in each immunohistochemical experiment to assist with interpretation of the results. This was accomplished by preabsorption with excess target proteins and by omission of the primary antibody to determine the amount of background generated from the detection assay. Tissue sections for 3-nitrotyrosine immunocytochemistry were preincubated for 6 hr at room temperature with either 20 mM nitrotyrosine or 1 mg/ml nitrated BSA containing ~30 μM nitrotyrosine to establish the specificity of antibody binding.

TUNEL

TUNEL staining was performed according to the method of Gavrieli et al. (1992) with minor modifications. Frozen tissue sections were fixed in 4% paraformaldehyde (Sigma, St. Louis, MO) and then washed in PBS (0.1 M, pH 7.4; Poly Scientific). The sections were treated with 10 μg/ml proteinase K (Boehringer Mannheim) at room temperature (RT) for 5 min and then washed in PBS. Sections were post-fixed in 4% paraformaldehyde for 15 min and then washed in PBS. Sections were immersed in TdT buffer (in mM: 30 Tris base, pH 7.2, 140 sodium cacodylate, and 1 cobalt chloride) for 5 min three times and then incubated with TdT buffer (974 μl) containing TdT enzyme (8 μl, Boehringer Mannheim) and biotinylated dUTP (10 μl, Boehringer Mannheim) for 60 min at 37°C. The reaction was terminated by NaCl (300 mM) and sodium citrate (30 mM) for 15 min at 25°C. Sections were then washed in PBS, followed by immersion in 1% H_2O_2 (Sigma) in PBS for 10 min at RT, and then rinsed in PBS for 5 min three times. The reaction product was visualized with a peroxidase standard Vectastain ABC kit (Vector Laboratories, Burlingame, CA) and diaminobenzidine (Sigma). For negative controls, sections were incubated without enzyme or biotinylated dUTP. Positive controls were immersed in DNase I (5 μl/5 ml of distilled water, Boehringer Mannheim) for 10 min at RT, before equilibration in TdT buffer.

TUNEL-positive cell counting

Terminal transferase labels 3′-DNA nicks, which are not specific for oligonucleosomal damage. Moreover, internucleosomal DNA breakdown can occur in necrotic cells (Grasl-Kraupp et al., 1995; vanLookeren-Campagne and Gill, 1996). Therefore, we used both morphological and histochemical (TUNEL positivity) criteria to classify

cells as apoptotic (Li et al., 1995a; Charriaut-Marlangue et al., 1996) and excluded from counting those cells showing features of necrosis. The cells classified as apoptotic were TUNEL-positive and showed condensed, occasionally fragmented nuclei with clumped chromatin but without cytoplasmic staining. Necrotic cells showed weak, diffuse DAB-positive cytoplasmic staining with or without a condensed and fragmented nucleus. Apoptotic cells were counted in a single tissue section at the largest lesion diameter within a preselected 100-μm-wide band (~2.5 mm; see Fig. 3*A*).

DNA fragmentation

Because TUNEL staining may not differentiate internucleosomal versus random DNA breakdown, we studied DNA fragmentation on agarose gels. Nonspecific DNA damage as well as internucleosomal DNA breaks were studied at 12, 24, and 48 hr and 7 d after NMDA injection (20 nmol) in SV129 mice ($n = 4$ at each time point) and 48 hr after NMDA in $nNOS^{+/+}$ and $nNOS^{-/-}$ littermates ($n = 3$ each). Brains were rapidly removed, and 2-mm-thick coronal slices were cut. The second slice containing both cortex and striatum was used for analysis after separating the hemispheres.

DNA was isolated (Puregene Systems, Minneapolis, MN), treated with DNase-free RNase (Boehringer Mannheim, Indianapolis, IN), and extracted by phenol/chloroform. The DNA was precipitated in 0.1 × volume of 3 M sodium acetate and 2.5 × volume of ice-cold 100% ethanol followed by incubation at −70°C for at least 60 min. The DNA was pelleted at 15,000 × *g* for 30 min at 4°C, washed with 80% ethanol, and air-dried for 30 min with tubes inverted. The pellets were resuspended in 25 ml of sterile water, and DNA concentration was determined by absorbance using the Christian and Warburg coefficient.

DNA damage was assessed by a radioactive end-labeling method by terminal transferase (Tilly and Hsueh, 1993) with minor modifications (Hara et al., 1997b). The DNA samples were labeled together with [α-^{32}P]dideoxy-ATP (3000 μCi mmol^{-1}; Amersham, Oakville, Ontario, Canada) and 25 U of terminal transferase (Boehringer Mannheim) in a final volume of 50 μl. The reaction was stopped by addition of 5 μl of 0.25 M EDTA, pH 8.0. Labeled DNA was separated from unincorporated radionucleotide by adding 0.2 volume 10 M ammonium acetate and 3 volume ice-cold 100% ethanol and incubating at −70°C for 60 min together with 50 μg of yeast tRNA (2 μl of a 25 mg/ml stock) to reduce background. The DNA was pelleted by centrifugation at 15,000 × *g* at 4°C for 30 min, washed with 80% ethanol, and allowed to air dry for 30 min with tubes inverted. The pellets were resuspended in 20 μl Tris-EDTA buffer. The labeled DNA samples were electrophoresed in a 2% agarose gel (agarose 3:1; Amresco, Solon, OH) at 50 V for 3.5 hr. The gels were placed on several sheets of Whatman (Maidstone, UK) 3M chromatography paper and dried in a slab gel dryer (model 224; Bio-Rad, Rockville Centre, NY) for 3–4 hr without heat. Dried gels were sealed in a plastic bag and exposed to Kodak (Rochester, NY) X-Omat films.

In vitro *receptor autoradiography*

We measured the density and distribution of glutamate receptors to determine whether differences in NMDA-induced toxicity were related to changes in glutamate receptor density. We assessed all three ionotropic glutamate receptor subtypes, because NMDA causes glutamate release and secondary AMPA and kainate receptor activation.

Mice were anesthetized with halothane and decapitated. The brains were quickly removed, frozen in liquid N_2, and kept at −80°C until used. Ten-micrometer sections were cut with a cryostat–microtome and thaw-mounted onto gelatin-coated slides. The slides were brought from −80°C to room temperature 30 min before the autoradiographic experiments.

NMDA receptors. Slides were preincubated three times for 15 min each at RT in 50 mM Tris·HCl, pH 7.5, and incubated for 60 min at 4°C in buffer containing 5 nM [^{3}H]D,L-(E)-2-amino-4-propyl-5-phosphono-3-pentanoic acid (CGP-39653) (44.5 Ci/mmol; DuPont NEN, Boston, MA). Nonspecific binding was assessed by the addition of 100 μM glutamate. Slides were washed four times for 15 sec each in ice-cold buffer, dipped in ice-cold distilled water, dried under a stream of cold air, and exposed to ^{3}H-Hyperfilms (Amersham) for 1 month.

AMPA receptors. Slides were preincubated three times for 15 min each at RT in (in mM) 50 Tris·acetate, 100 KSCN, and 2.5 $CaCl_2$, pH 7.3, and incubated for 45 min at 4°C in buffer containing 9 nM [^{3}H]AMPA (45.3 Ci/mmol, DuPont NEN). Nonspecific binding was assessed by the addition of 1 mM glutamate. Slides were washed three times for 10 sec each in ice-cold buffer, dipped in ice-cold distilled water, dried under a stream of cold air, and exposed to ^{3}H-Hyperfilms (Amersham) for 1 month.

Kainate receptors. Slides were preincubated three times for 15 min each at RT in 50 mM Tris·acetate, pH 7.4, and incubated for 45 min at 4°C in buffer containing 12 nM [^{3}H]kainate (58.0 Ci/mmol, Dupont NEN). Nonspecific binding was assessed by the addition of 1 μM kainate. Slides were washed three times for 10 sec each in ice-cold buffer, dipped in ice-cold distilled water, dried under a stream of cold air, and exposed to ^{3}H-Hyperfilms (Amersham) for 6 weeks.

Autoradiograms were analyzed by comparing the optical density of the film over specific brain regions with that over tritiated standards (Amersham) using a computerized system (M4, Imaging Research). Data are given in nanocuries of bound radioligand per milligram of tissue.

Data analysis. The data are expressed as mean ± SEM. Two-way ANOVA for repeated measures or one-way ANOVA followed by Tukey's multiple comparison test were used to compare three or more groups. Student's *t* test was used to compare two groups.

RESULTS

NMDA lesions in wild-type and nNOS-deficient mice

Intrastriatal microinjections of NMDA consistently produced well delineated lesions. The lesions were usually located approximately at the level of bregma and confined to the striatum except at the highest dose (20 nmol) when the adjacent cortex was affected. In preliminary experiments using SV129 mice, we determined at the light microscopic level that the loss of striatal neurons started as early as 3 hr, without significant tissue edema, and became grossly recognizable 6 hr after NMDA injection. At 12–24 hr, there was marked edema and pallor, with a much lower cell density and the beginning of glial proliferation. At 24 and 48 hr, the lesion contained many reactive glia and necrotic as well as shrunken cells with pyknotic, densely stained nuclei, particularly at the margins. Remnants of fragmented cells (apoptotic bodies), mainly distributed along the lesion boundary, were observed only occasionally at 48 hr but frequently at 7 d. The lesions were characterized by marked gliosis at 7 d. Maximum lesion volume was reached at 6–48 hr. For all subsequent experiments, animals were killed at 48 hr after NMDA injection.

The NMDA receptor antagonist MK-801 (4 mg/kg, i.p.) completely prevented lesion development (19.5 ± 3.7 and 0 ± 0 mm^3 in vehicle and MK-801 groups, respectively, after 10 nmol of NMDA) when tested in SV129 mice ($n = 5$).

NMDA-induced lesions were 45% smaller in $nNOS^{-/-}$ mice ($nNOS^{+/+}$, 11.7 ± 1.7 mm^3; $n = 8$; $nNOS^{-/-}$, 6.4 ± 1.8 mm^3; $n = 7$; $p < 0.05$). In addition to smaller lesions, $nNOS^{-/-}$ mice showed more sparing of neurons within the lesion bed compared with $nNOS^{+/+}$ mice.

Effects of 7-NI on NMDA toxicity

7-NI (50 mg/kg, i.p.) was used to evaluate the importance of neuronal NOS in SV129 mice. 7-NI decreased lesion volume by ~32% (30.0 ± 2.9 mm^3; $n = 7$) compared with vehicle injection (43.8 ± 5.4 mm^3; $p < 0.01$; $n = 6$).

3-Nitrotyrosine production after NMDA microinjection

Brain levels of 3-nitrotyrosine were measured as a reflection of peroxynitrite formation. 3-nitrotyrosine levels increased by ~100% in wild-type mice 1 hr after NMDA injection (Fig. 1*A*). The levels were at baseline 6 ($n = 6$) and 24 ($n = 6$) hr later. 3-Nitrotyrosine levels did not change in $nNOS^{-/-}$ mice.

We further evaluated the 3-nitrotyrosine production by immunohistochemistry. Twelve hours after NMDA injection, striatal lesions were observed within the NMDA injection site in both $nNOS^{-/-}$ and wild-type mice (Fig. 2*A,B*); the lesion size was smaller in the $nNOS^{-/-}$ mice and was primarily restricted to the injection site. There was a marked increase in immunohistochemical expression of 3-nitrotyrosine within the lesioned striatum of

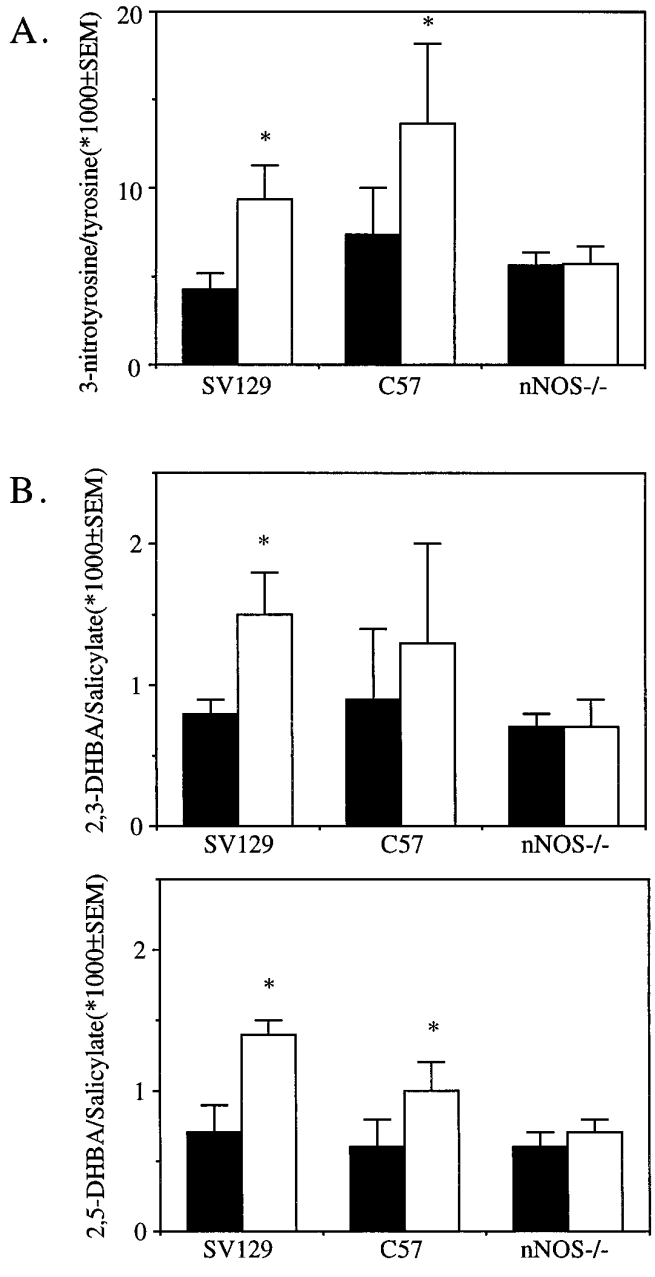

Figure 1. Production of 3-nitrotyrosine and 2,3- and 2,5-DHBA 1 hr after intrastriatal injection of NMDA in wild-type (SV129, $n = 11$; C57/B6, $n = 5$) and nNOS$^{-/-}$ ($n = 9$) mice. *A*, NMDA (20 nmol) significantly increased striatal 3-nitrotyrosine levels in both wild-type strains but not in nNOS$^{-/-}$ mice (*open bars*) 1 hr after injection, compared with the contralateral unlesioned (*filled bars*) striatum. 3-Nitrotyrosine was measured electrochemically. *B*, NMDA (20 nmol) increased striatal 2,3- and 2,5-DHBA production by ~100% and 50% in SV129 and C57BL/6 mice, respectively (*open bars*), 1 hr after injection, compared with the contralateral unlesioned (*filled bars*) striatum. Levels in nNOS$^{-/-}$ mice showed no change. Using the salicylate OH•-trapping method, 2,3- and 2,5-DHBA were measured by HPLC. $^*p < 0.05$ versus contralateral hemisphere. Error bars indicate ±SEM.

wild-type mice (Fig. 2*C*). Immunostaining was present in both neurons and the surrounding neuropil (Fig. 2*E*). 3-Nitrotyrosine immunoreactivity was not observed in nonlesioned brain areas. In contrast, 3-nitrotyrosine immunolabel was not present in the lesioned striatal areas of nNOS$^{-/-}$ mice (Fig. 2*D,F*). 3-Nitrotyrosine immunoreactivity was completely eliminated from the tissue sections by preincubation using nitrotyrosine or nitrotyrosine bovine serum albumin.

Hydroxyl radical (OH•) production after NMDA

We examined striatal levels of 2,3- and 2,5-DHBA as a measure of OH• radical formation. NMDA injection significantly increased OH• radical production in the ipsilateral striatum after 1 hr in both C57BL/6J and SV129 mice. 2,3-DHBA levels returned to baseline 6 ($n = 6$) and 24 ($n = 6$) hr after NMDA in SV129 mice, whereas 2,5-DHBA levels remained elevated for 24 hr (data not shown). One hour after NMDA injection, 2,3- and 2,5-DHBA levels did not increase in nNOS$^{-/-}$ mice (Fig. 1*A,B*).

DNA fragmentation

To assess the importance of apoptosis to lesion development, we examined oligonucleosomal DNA breakdown (laddering) after NMDA injection. Oligonucleosomal DNA breakdown as well as total DNA fragmentation was observed beginning at 12–24 hr and persisted at 48 hr (Fig. 3*A*) and 7 d in wild-type mice. nNOS$^{-/-}$ mice had lower total as well as oligonucleosomal DNA breakdown compared with wild-type littermates 48 hr after NMDA injection (Fig. 3*B*).

We counted the number of TUNEL-positive cells after NMDA microinjections ($n = 4$ per time point at 3, 6, 12, 24, and 48 hr and 7 d). There were no TUNEL-positive cells 3 or 6 hr after NMDA injection, even though histopathological evidence for necrosis started as early as 3 hr. Positively stained cells first appeared at 12 hr and were distributed relatively homogenously throughout the lesion. Over the subsequent 36 hr, TUNEL-positive cells were noted primarily at the margins of the lesion, and the cells acquired a more characteristic apoptotic morphology (more fragmented nuclei and apoptotic bodies; Fig. 4*D,E*). The total number of TUNEL-positive cells did not increase significantly beyond 48 hr. However, their distribution shifted further toward the periphery, so that at 7 d, TUNEL-positive cells formed a dense ring at the outer rim of the lesion (Fig. 4*B*) and were also observed at the outside of the lesion margins when compared with adjacent H&E-stained sections. The density of TUNEL-positive cells in general was higher in the medial compared with the lateral striatum (Fig. 4*B,C*).

At 48 hr, ~30% of TUNEL-positive cells showed diffuse cytoplasmic staining and no clear nuclear or cytoplasmic border, more consistent with the appearance of necrotic cells. Approximately 10% of TUNEL-positive cells possessed nuclear fragmentation and chromatin condensation superimposed on a diffuse cytoplasmic staining, thus exhibiting both apoptotic and necrotic characteristics.

The morphology of TUNEL-positive cells in nNOS$^{-/-}$ mice ($n = 6$) did not differ from that in the wild-type strain ($n = 7$), although the density of apoptotic neurons in the lesion was less in nNOS$^{-/-}$ mice (406 ± 28 and 280 ± 8 neurons/mm^2 in nNOS$^{+/+}$ and nNOS$^{-/-}$ mice, respectively; $p < 0.01$). The differences were pronounced in the lateral half of the lesion only (Fig. 4*C*).

Glutamate receptor autoradiography

Because glutamate receptor density and/or distribution could contribute to the observed resistance to NMDA in nNOS$^{-/-}$ mice, we performed NMDA, AMPA, and kainate receptor autoradiography in coronal brain sections from three strains (Table 1). The data from knock-out mice lacking type III NOS are also listed for comparison. The highest density binding for all three ligands was in the hippocampus. Intense labeling was

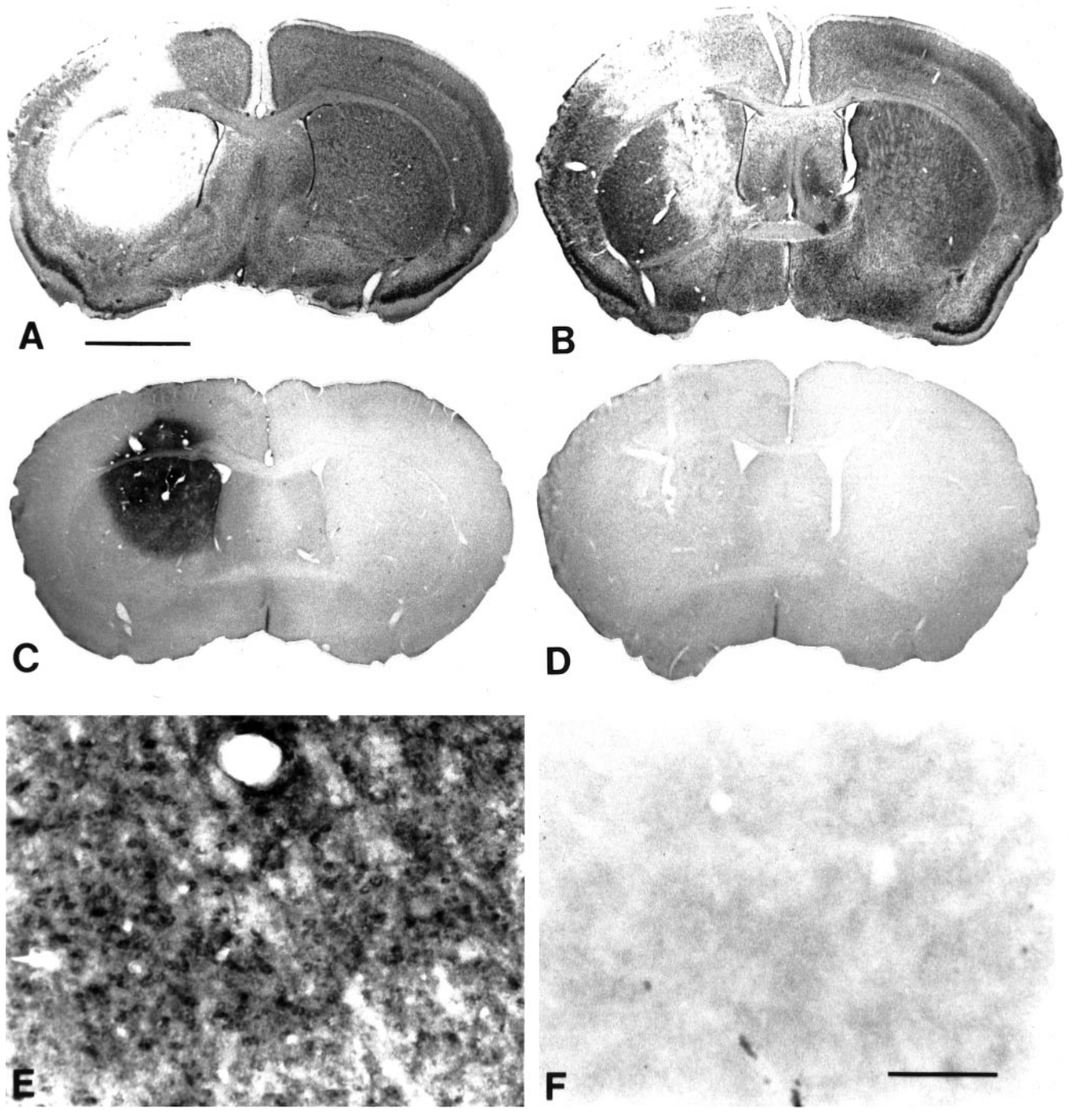

Figure 2. Histopathology and 3-nitrotyrosine immunohistochemistry of striatal NMDA lesions in wild-type (*A*, *C*, *E*) and nNOS$^{-/-}$ (*B*, *D*, *F*) mice 12 hr after injection. Nissl staining of NMDA-lesioned brains identifies the extent of the damage (staining pallor) in both the wild-type (*A*) and nNOS$^{-/-}$ mice (*B*). In adjacent cut sections, expression of 3-nitrotyrosine immunoreactivity is markedly increased in the wild-type mouse (*C*, *E*), with no immunolabel observed within the nNOS$^{-/-}$ mouse (*D*, *F*). 3-Nitrotyrosine immunoreactivity is found in both neuron soma and neuropil in the wild-type animals. Scale bars: *A*, 2 mm, same for *B–D*; *F*, 200 μm, same for *E*.

also observed in the striatum and neocortex. The density of NMDA receptors was higher in the lateral striatum compared with the medial striatum in all strains. Strain differences were not observed for any of the three ligands, except that the density of AMPA receptors in the CA1 region of SV129 mice was higher than in C57BL/6J mice. It should be noted that the listed values were obtained at nonsaturating ligand concentrations; the validity of the comparisons thus relies on the assumption that the affinity of the receptors for their respective ligands does not differ among strains.

DISCUSSION

We demonstrated that type I NOS gene knock-out or pharmacological inhibition by 7-nitroindazole confers neuroprotection against NMDA receptor-mediated toxicity in striatum. We

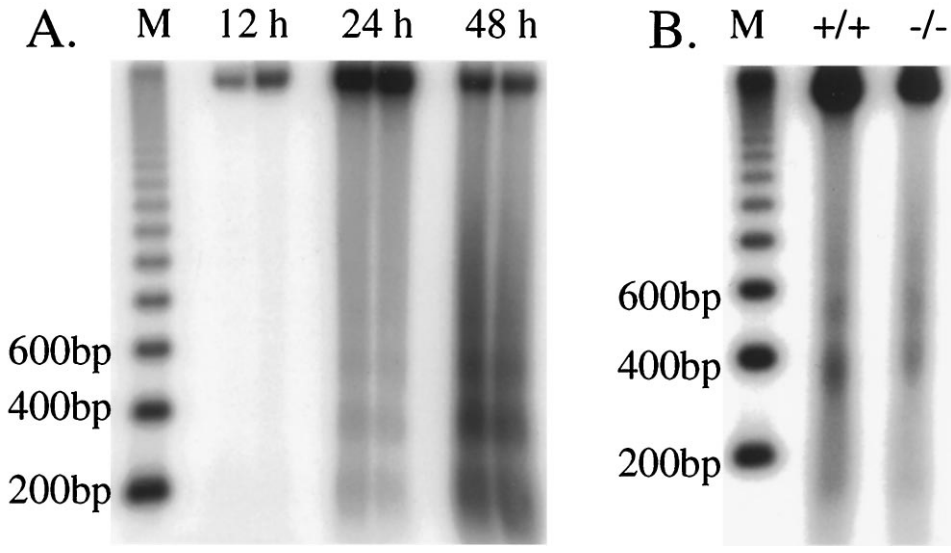

Figure 3. Autoradiograms of agarose gels showing DNA breakdown after intrastriatal NMDA injection (20 nmol). Brains were removed rapidly, and 2-mm-thick coronal slices were cut. DNA was isolated from the second slice containing both cortex and striatum, and a [^{32}P]dideoxy-ATP end-labeling method with terminal transferase was performed. *A*, DNA breakdown both in the form of nonspecific fragmentation (smearing) and oligonucleosomal breakdown (laddering) appears at 12–24 hr and intensifies 48 hr after NMDA in SV129 mice. Each *lane* contains tissue obtained from different animals killed at 12, 24, and 48 hr after NMDA injection. *B*, Both nonspecific DNA fragmentation and oligonucleosomal breakdown are observed to a lesser extent in nNOS$^{-/-}$ compared with nNOS$^{+/+}$ littermates 48 hr after NMDA. The gel is representative of three independent experiments. *M*, Molecular weight marker.

also showed that the mechanism was probably related to a deficiency of NO$^{\bullet}$ and its products, as reflected by lower levels of free 3-nitrotyrosine as well as 2,3- and 2,5-DHBA and nitrotyrosine immunostaining. Our findings suggest that apoptosis may be an important delayed mechanism of cell death after NMDA receptor activation, observed at 12 hr after injection but not before. The findings are consistent with results of previous *in vivo* studies showing that nNOS deficiency confers resistance to injury after permanent (Huang et al., 1994) or transient focal (Hara et al., 1996) or global cerebral ischemia (Panahian et al., 1996) or after striatal malonate injection (Schulz et al., 1996). The findings also agree with results showing that cortical cells cultured from nNOS$^{-/-}$ mice are resistant to NMDA toxicity (Dawson et al., 1996), or that inhibition of nNOS by 7-nitroindazole protected against focal ischemia (Yoshida et al., 1994) or NMDA-induced toxicity in rats (Schulz et al., 1995). The extent of protection in nNOS$^{-/-}$ mice (~45%) was greater than that achieved by 7-NI (32%), probably because the degree of NOS inhibition obtained using knock-out technology is greater and longer-lasting than after drug administration.

The precise mechanism(s) by which NO$^{\bullet}$ mediates neurotoxicity is not clear, and many mechanisms have been proposed, including DNA damage (Wink et al., 1991), energy depletion attributable to poly(ADP-ribose) polymerase activation (Berger, 1985; Zhang, 1994), and inhibition of mitochondrial respiration (Stadler et al., 1991; Radi et al., 1994). One of the most attractive mechanisms involves peroxynitrite formation, which is initiated via NMDA receptor activation, intracellular Ca^{2+} increase, and augmented NO$^{\bullet}$ synthesis (Garthwaite et al., 1988). Peroxynitrite ($ONOO^-$) is formed by the reaction of NO$^{\bullet}$ with $O_2^{\bullet -}$ (Lafon-Cazal et al., 1993; Dykens, 1994), and this complex rapidly decomposes into $NO_2^{\bullet}$ and hydroxyl radical (OH$^{\bullet}$) or a reactive intermediate with OH$^{\bullet -}$-like activity (Crow et al., 1994). Hydroxyl radical is a highly reactive species that leads to oxidation of sulfhydryl groups, lipids, DNA, and proteins (Beckman et al., 1996). Peroxynitrite can directly inhibit glutamate transporters (Trotti et al., 1996) or produce nitronium ions, causing irreversible nitration of tyrosine residues in proteins (Beckman et al., 1996). Protein tyrosine nitration may contribute to NO$^{\bullet}$ toxicity by reducing phosphorylation by tyrosine kinases (Beckman et al., 1996) or targeting nitrated proteins for degradation (Gow et al., 1996).

We studied brain levels of free 3-nitrotyrosine as an indirect measure of protein tyrosine nitration and as a footprint of peroxynitrite formation during NMDA receptor activation. Compared with robust increases in wild-type mice, brain levels of 3-nitrotyrosine and OH$^{\bullet}$ radical did not rise in nNOS$^{-/-}$ brains, suggesting that the reaction of NO$^{\bullet}$ with $O_2^{\bullet -}$ is a major pathway that generates peroxynitrite and OH$^{\bullet}$ radical-like activity in brain after NMDA receptor activation. Nevertheless, $O_2^{\bullet -}$ can induce neurotoxicity independent of its reaction with NO$^{\bullet}$ (Chan, 1996), because superoxide dismutase can still protect cortical cell cultures from nNOS$^{-/-}$ mice against NMDA toxicity (Dawson et al., 1996). In the same study, sodium nitroprusside and 3-(4-morpholinyl)-sydnone imine hydrochloride were equally toxic to cultured cells from wild-type and nNOS$^{-/-}$ mice, confirming the importance of a deficiency of NO$^{\bullet}$ synthesis as a mechanism of resistance to cytotoxicity. Despite greatly reduced NO$^{\bullet}$ and OH$^{\bullet}$ radical production, the protection was ~50% in nNOS$^{-/-}$ mice, suggesting a role for additional mechanisms, such as acute neuronal swelling and lysis, and $O_2^{\bullet -}$ toxicity (Chan, 1996; Kamii et al., 1996).

Basal 3-nitrotyrosine levels in wild-type and NOS$^{-/-}$ mice were measurable in the nonlesioned striatum as well, suggesting alternative pathways for nitrotyrosine formation in both normal wild-type and nNOS$^{-/-}$ brains that may be independent of NMDA-induced NO formation. Of interest, alternative splice variants of NOS have been reported that generate NO *in vitro* but lack the PDZ-containing domain and potential coupling to the NMDA receptor (Brenman et al., 1996; Eliasson et al., 1997). However, NOS activity in nNOS$^{-/-}$ brains was very low, measured by the conversion of [^{3}H]L-arginine to [^{3}H]L-citrulline *in vitro* (Hara et al., 1996). The time course of 3-nitrotyrosine and 2,3-DHBA production was similar, suggesting that NO$^{\bullet}$ and hydroxyl radical synthesis occurs predominantly within the first hour. The elevation in 3-nitrotyrosine was no longer detectable 6 hr after NMDA injection, suggesting that the removal of free 3-nitrotyrosine can be fairly rapid. In contrast, robust staining for nitrotyrosine was observed immunohistochemically 12 hr after NMDA injection in wild-type striatum, suggesting a much longer half-life for nitrotyrosine found in proteins (Beckman et al., 1996). 2,5-DHBA levels may be more indicative of cytochrome P-450 activity (Halliwell et al., 1991) and remained elevated in wild-type brain up to 24 hr.

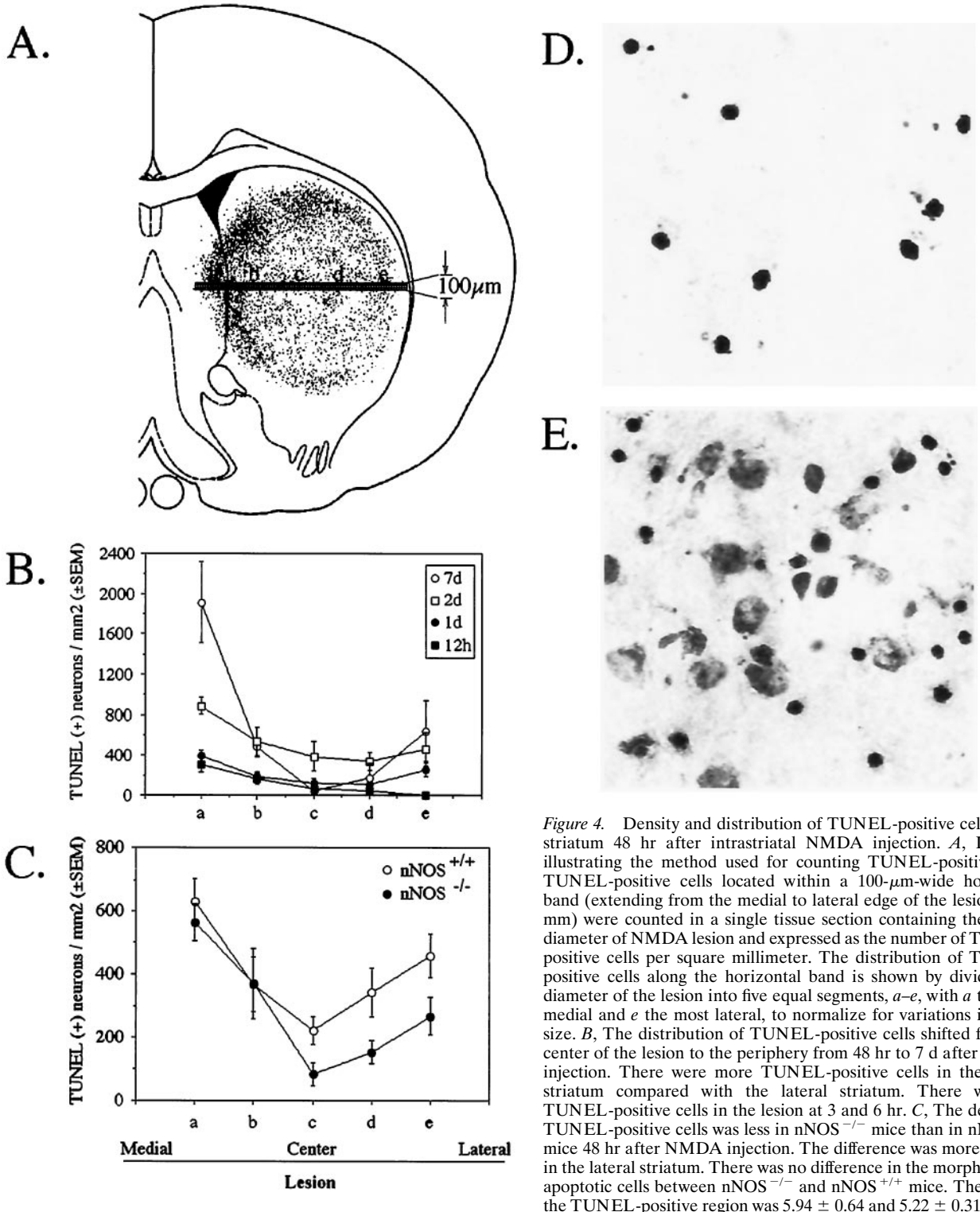

Figure 4. Density and distribution of TUNEL-positive cells in the striatum 48 hr after intrastriatal NMDA injection. *A*, Diagram illustrating the method used for counting TUNEL-positive cells. TUNEL-positive cells located within a 100-μm-wide horizontal band (extending from the medial to lateral edge of the lesion, ~2.5 mm) were counted in a single tissue section containing the largest diameter of NMDA lesion and expressed as the number of TUNEL-positive cells per square millimeter. The distribution of TUNEL-positive cells along the horizontal band is shown by dividing the diameter of the lesion into five equal segments, *a–e*, with *a* the most medial and *e* the most lateral, to normalize for variations in lesion size. *B*, The distribution of TUNEL-positive cells shifted from the center of the lesion to the periphery from 48 hr to 7 d after NMDA injection. There were more TUNEL-positive cells in the medial striatum compared with the lateral striatum. There were no TUNEL-positive cells in the lesion at 3 and 6 hr. *C*, The density of TUNEL-positive cells was less in nNOS$^{-/-}$ mice than in nNOS$^{+/+}$ mice 48 hr after NMDA injection. The difference was more marked in the lateral striatum. There was no difference in the morphology of apoptotic cells between nNOS$^{-/-}$ and nNOS$^{+/+}$ mice. The area of the TUNEL-positive region was 5.94 ± 0.64 and 5.22 ± 0.31 mm^2 in nNOS$^{+/+}$ and nNOS$^{-/-}$ groups, respectively ($p > 0.05$). The distances from the center of the TUNEL-positive area to the midline and to the dorsal cortical surface were similar in both nNOS$^{+/+}$ and nNOS$^{-/-}$ groups (data not shown). Error bars indicate ±SEM. *D*, Photomicrograph of TUNEL-stained section, taken from the periphery of the lesion, 48 hr after NMDA injection in an SV129 mouse, illustrating densely stained pyknotic nuclei with occasional apoptotic bodies. *E*, Photomicrograph of H&E-stained section, taken from a region similar to *D*, 48 hr after NMDA injection in an SV129 mouse. A wide variety of cellular morphology is observed, including necrotic as well as intact cells. Cells with pyknotic nuclei and occasional apoptotic bodies are observed along with necrotic cells. Cells with a normal morphology are also seen.

Table 1. Density and distribution of ionotropic glutamate receptor binding sites in mouse brain

	C57/B6	SV129	$nNOS^{-/-}$	$eNOS^{-/-}$
NMDA				
Cortex	9.85 ± 0.54	9.76 ± 0.51	9.01 ± 0.41	9.38 ± 0.50
Striatum (lateral)[a]	5.21 ± 0.36	5.44 ± 0.48	4.75 ± 0.26	4.98 ± 0.17
Striatum (medial)[a]	3.35 ± 0.28	3.58 ± 0.29	3.03 ± 0.19	3.23 ± 0.13
CA1	17.84 ± 0.67	15.78 ± 1.74	15.39 ± 1.05	16.91 ± 0.52
Cerebellum	2.93 ± 0.27	2.86 ± 0.23	2.56 ± 0.24	3.12 ± 0.08
KA				
Striatum[a]	7.52 ± 0.29	8.53 ± 0.56	8.22 ± 0.57	7.69 ± 0.22
Cortex (internal)[a]	8.20 ± 0.26	8.08 ± 0.59	7.95 ± 0.64	7.72 ± 0.20
Cortex (external)[a]	4.75 ± 0.23	5.07 ± 0.41	5.07 ± 0.39	5.08 ± 0.09
CA3	10.88 ± 0.39	10.90 ± 0.60	10.61 ± 0.57	10.57 ± 0.32
Cerebellum	5.27 ± 0.32	5.46 ± 0.34	4.82 ± 0.35	5.39 ± 0.20
AMPA				
Striatum (ventromedial)	8.64 ± 0.13	9.02 ± 0.44	9.19 ± 0.42	8.07 ± 0.35
Striatum (dorsolateral)	6.98 ± 0.23	6.97 ± 0.46	7.18 ± 0.38	6.39 ± 0.19
Cortex (internal)	6.54 ± 0.19	6.79 ± 0.40	6.79 ± 0.42	5.99 ± 0.13
Cortex (external)	7.96 ± 0.32	8.26 ± 0.47	7.74 ± 0.37	7.67 ± 0.29
CA1	11.69 ± 0.19	13.19 ± 0.36	12.30 ± 0.31	12.44 ± 0.38
Cerebellum	6.65 ± 0.21	6.840 ± 24	6.92 ± 0.32	6.30 ± 0.22

Densities of NMDA, kainate, and AMPA binding sites in different areas of control mice (C57/B6 and SV129) and mice lacking the neuronal ($nNOS^{-/-}$) or endothelial ($eNOS^{-/-}$) isoform of NOS. Values are given as nanocuries per milligram of tissue ± SEM (mean of six animals in each group). The sites were labelled using [^{3}H]CGP-39653, [^{3}H]kainate, and [^{3}H]AMPA, respectively, as described in Materials and Methods. For each region, the density of the relevant receptor was compared in the four strains, using ANOVA followed by Tukey's multiple range test (except in a few regions, which did not show equal variance and were thus compared using a Kruskal–Wallis test). The only significant difference was observed for AMPA binding sites in the hippocampus (CA1) of SV129 versus C57/B6 mice. ANOVA followed by Tukey's test also showed that the densities of NMDA binding sites in the lateral versus medial aspects of the striatum were significantly different (data not shown).

[a] Regions compared using a Kruskal–Wallis test.

NMDA-induced striatal cell loss and pallor were visible at 3 hr, and the lesion reached its maximum volume at 6 hr. Accompanying this early cell loss, 2,3-DHBA and 3-nitrotyrosine levels increased at 1 hr, completely recovered by 6 hr, and stayed at baseline levels until 24 hr, suggesting that $OH^{\bullet}$ radical and peroxynitrite formation takes place early after NMDA injection. On the other hand, *in situ* labeling of 3′-OH DNA breaks (TUNEL staining) and oligonucleosomal DNA breakdown (DNA laddering) were observed only after 12–24 hr and increased at 48 hr. The delayed onset of oligonucleosomal DNA breakdown, nuclear fragmentation, and chromatin condensation suggest that NMDA induces an initial cell loss (3–6 hr), followed many hours later by a form of death resembling apoptosis. The delayed onset probably indicates that one or more intervening steps initiate apoptosis after NMDA microinjection and receptor activation. In a recent study, inhibition of interleukin-1β-converting-enzyme decreased NMDA lesion size by 25% 48 hr after microinjection (Hara et al., 1997), further establishing the linkage between the two.

The stimulus for apoptotic cell death is unknown but probably depends in part on NMDA receptor-mediated Ca^{2+} influx and free radical formation (e.g., $NO^{\bullet}$, $O_2^{\bullet -}$, peroxynitrite, and $OH^{\bullet}$). Apoptosis can be observed in cortical or cerebellar granule cell cultures (Ankarcrona et al., 1995) after the addition of NMDA, especially at low concentrations (Bonfoco et al., 1995), or after intrastriatal injection (Ferrer et al., 1995; vanLookeren-Campagne et al., 1995; Qin et al., 1996). Direct application of $NO^{\bullet}$ or peroxynitrite can also trigger apoptotic cell death (Albina et al., 1993; Ratan et al., 1994; Bonfoco et al., 1995; Estevez et al., 1995; Lin et al., 1995; for review, see Nicotera et al., 1995; Palluy and Rigaud, 1996) possibly related to DNA damage (Inoue and Kawanishi, 1995; Salgo et al., 1995; Szabo, 1996; Tamir et al., 1996), an increase in *p53* gene expression (Messmer et al., 1994; Messmer and Brüne, 1996), or inhibition of mitochondrial respiration (Stadler et al., 1991; Radi et al., 1994; Wolvetang et al., 1994; Behrens et al., 1995; Cassina and Radi, 1996; Poderoso et al., 1996). Consistent with these findings, blockade of superoxide dismutase-1 by antisense oligonucleotides causes apoptosis, which is decreased by also blocking $NO^{\bullet}$ (and probably peroxynitrite) formation (Troy et al., 1996).

TUNEL-positive cells were evenly distributed within the lesion at 1 d. Time-dependent studies showed that the density of TUNEL-positive cells gradually increased in the periphery and decreased in the center of the lesion. Hence, TUNEL-positive cells were distributed predominantly within the periphery at 7 d and resembled the pattern reported in focal cerebral ischemia (Li et al., 1995a). Relatively lower NMDA concentrations in the periphery versus core might explain the distribution of positive cells at the lesion margin, as observed in the penumbra of an ischemic lesion (Li et al., 1995a). In fact, damage caused by mild ischemia can be successfully prevented by drugs that block apoptosis, such as cycloheximide (Du et al., 1996) or cysteine protease inhibitors (Endres et al., 1997). Unlike NMDA lesions, however, TUNEL-positive cells and DNA laddering appear within a few hours after 2 hr middle cerebral artery occlusion (Li et al., 1995b), suggesting additional mechanisms that differentiate ischemia and excitotoxicity.

Regions of high NMDA receptor density may be linked more closely to necrotic than apoptotic cell death, because the density of NMDA receptor binding sites, higher in lateral than medial striatum, contrasts with the higher density of TUNEL-positive

cells found within medial striatum. The data from nNOS $^{-/-}$ mice suggest that apoptotic cell death may be linked to NO$^{\bullet}$ in regions with a high density of NMDA receptors. These apparent discrepancies point to mechanisms in addition to NOS activation linking NMDA receptor occupancy and development of delayed cell death, at least within medial striatum. Measuring levels of NO$^{\bullet}$ within medial and lateral striatum may help clarify this issue, because the ability of NO$^{\bullet}$ to promote apoptosis or necrosis may well be concentration-dependent (Bonfoco et al., 1995).

In conclusion, our study demonstrates that NO$^{\bullet}$ synthesized by the neuronal NOS isoform is an important mediator in NMDA receptor-mediated toxicity and promotes apoptosis as a delayed and probably secondary mechanism of cell death.

REFERENCES

Albina JE, Cui S, Mateo RB, Reichner S (1993) Nitric oxide-mediated apoptosis in murine peritoneal macrophages. J Immunol 150:5080–5085.

Ankarcrona M, Dypbukt JM, Bonfoco E, Zhivotovsky B, Orrenius S, Lipton SA, Nicotera P (1995) Glutamate-induced neuronal death: a succession of necrosis or apoptosis depending on mitochondrial function. Neuron 15:961–973.

Beckman JS, Ye YZ, Chen J, Conger JA (1996) The interactions of nitric oxide with oxygen radicals and scavengers in cerebral ischemic injury. In: Advances in neurology: cellular and molecular mechanisms of ischemic brain damage (Siesjö BK, Wieloch T, eds), pp 339–354. Philadelphia: Lippincott-Raven.

Behrens MI, Koh J, Canzoniero LMT, Sensi SL, Csernansky CA, Choi DW (1995) 3-Nitropropionic acid induces apoptosis in cultured striatal and cortical neurons. NeuroReport 6:545–548.

Berger NA (1985) Poly(ADP-ribose) in the cellular response to DNA damage. Radiat Res 101:4–15.

Bonfoco E, Krainc D, Ankarcrona M, Nicotera P, Lipton SA (1995) Apoptosis and necrosis: two distinct events induced, respectively, by mild and intense insults with *N*-methyl-D-aspartate or nitric oxide/superoxide in cortical cell cultures. Proc Natl Acad Sci USA 92:7162–7166.

Bredt DS, Snyder SH (1990) Isolation of nitric oxide synthetase, a calmodulin requiring enzyme. Proc Natl Acad Sci USA 87:682–685.

Brenman JE, Chao DS, Gee SH, McGee AW, Craven SE, Santillano DR, Wu Z, Huang F, Xia H, Peters MF, Froehner SC, Bredt DS (1996) Interaction of nitric oxide synthase with the postsynaptic density protein PSD-95 and α1-syntrophin mediated by PDZ domains. Cell 84:757–767.

Cassina A, Radi R (1996) Differential inhibitory action of nitric oxide and peroxynitrite on mitochondrial electron transport. Arch Biochem Biophys 328:309–316.

Chan PH (1996) Role of oxidants in ischemic brain damage. Stroke 24:1124–1129.

Charriaut-Marlangue C, Aggoun-Zouaoui D, Represa A, Ben-Ari Y (1996) Apoptotic features of selective neuronal death in ischemia, epilepsy, and gp120 toxicity. Trends Neurosci 19:109–114.

Connop BP, Boegman RJ, Jhamandas K, Beninger RJ (1995) Excitotoxic action of NMDA agonists on nigrostriatal dopaminergic neurons: modulation by inhibition of nitric oxide synthesis. Brain Res 676:124–132.

Crow JP, Spruell C, Chen J, Gunn C, Ischiropoulos H, Tsai M, Smith CD, Radi R, Koppenol WH, Beckman JS (1994) On the pH dependent yield of hydroxyl radical products from peroxynitrite. Free Radic Biol Med 16:331–338.

Dalkara T, Yoshida T, Irikura K, Moskowitz MA (1994) Dual role of nitric oxide in focal cerebral ischemia. Neuropharmacology 33:1447–1452.

Dawson VL, Dawson TM, London ED, Bredt DS, Snyder SH (1991) Nitric oxide mediates glutamate neurotoxicity in primary cortical cultures. Proc Natl Acad Sci USA 88:6368–6371.

Dawson VL, Kizushi VM, Huang PL, Snyder SH, Dawson TM (1996) Resistance to neurotoxicity in cortical cultures from neuronal nitric oxide synthase-deficient mice. J Neurosci 16:2479–2487.

Du C, Hu R, Csernansky CA, Hsu CY, Choi D (1996) Very delayed infarction after mild focal cerebral ischemia: a role for apoptosis? J Cereb Blood Flow Metab 16:195–201.

Dykens JA (1994) Isolated cerebral and cerebellar mitochondria produce free radicals when exposed to elevated Ca^{2+} and Na^{+}: implications for neurodegeneration. J Neurochem 63:584–591.

Eliasson MJL, Blackshaw S, Schell MJ, Snyder SH (1997) Neuronal nitric oxide synthase alternatively spliced forms: prominent functional localizations in the brain. Proc Natl Acad Sci USA 94:3396–3401.

Endres M, Namura S, Hara H, Waeber C, Moskowitz MA (1997) Attenuation of delayed cell death during mild ischemia by the interleukin-1β-converting-enzyme family inhibitor Z-VAD.FMK. J Cereb Blood Flow Metab 17 [Suppl 1]:S251.

Estevez AG, Radi R, Barbeito L, Shin JT, Thompson JA, Beckman JS (1995) Peroxynitrite-induced cytotoxicity in PC12 cells: evidence for an apoptotic mechanism differentially modulated by neurotrophic factors. J Neurochem 65:1543–1550.

Ferrante RJ, Kowall NW, Cipolloni PB, Storey E, Beal MF (1993) Excitotoxin lesions in primates as a model for Huntington's disease: histopathologic and neurochemical characterization. Exp Neurol 119:46–71.

Ferrer I, Martin F, Serrano T, Reiriz J, Perez-Navarro E, Alberch J, Macaya A, Planas AM (1995) Both apoptosis and necrosis occur following intrastriatal administration of excitotoxins. Acta Neuropathol (Berl) 90:504–510.

Floyd RA, Watson JJ, Wong PK (1984) Sensitive assay of hydroxyl free radical formation utilizing high pressure liquid chromatography with electrochemical detection of phenol and salicylate hydroxylation products. J Biochem Biophys Methods 10:221–235.

Garthwaite J, Charles SL, Chess-Williams R (1988) Endothelium-derived relaxing factor release on activation of NMDA receptors suggests role as intercellular messenger in the brain. Nature 336:385–388.

Gavrieli Y, Sherman Y, Ben-Sasson SA (1992) Identification of programmed cell death *in situ* via specific labeling of nuclear DNA fragmentation. J Cell Biol 119:493–501.

Globus MYT, Prado R, Sanchez-Ramos J, Zhao W, Dietrich WD, Busto R, Ginsberg MD (1995) A dual role for nitric oxide in NMDA-mediated toxicity in vivo. J Cereb Blood Flow Metab 15:904–913.

Gow AJ, Duran D, Malcolm S, Ischiropoulos H (1996) Effects of peroxynitrite-induced protein modifications on tyrosine phosphorylation and degradation. FEBS Lett 385:63–66.

Grasl-Kraupp B, Ruttkay-Nedecky B, Koudelka H, Bukowska K, Bursch W, Schulte-Hermann R (1995) *In situ* detection of DNA (TUNEL assay) fails to discriminate among apoptosis, necrosis, and autolytic cell death: a cautionary note. Hepatology 21:1465–1468.

Halliwell B, Kaur H, Ingelman-Sundberg M (1991) Hydroxylation of salicylate as an assay for hydroxyl radicals: a cautionary note. Free Radic Biol Med 10:439–441.

Hara H, Puang PL, Panahian N, Fishman MC, Moskowitz MA (1996) Reduced brain edema and infarction volume in mice lacking the neuronal isoform of nitric oxide synthase after transient MCA occlusion. J Cereb Blood Flow Metab 16:605–611.

Hara H, Friedlander RM, Gagliardini V, Ayata C, Fink K, Huang Z, Shimizu-Sasamata M, Yuan J, Moskowitz MA (1997a) Inhibition of interleukin 1β-converting enzyme family proteases reduces ischemic and excitotoxic neuronal damage. Proc Natl Acad Sci USA 94:2007–2012.

Hara H, Fink K, Endres M, Friedlander RM, Gagliardini V, Yuan J, Moskowitz MA (1997b) Attenuation of transient focal cerebral ischemic injury in transgenic mice expressing a mutant ICE inhibitory protein. J Cereb Blood Flow Metab 17:370–375.

Huang PL, Dawson TM, Bredt DS, Snyder SH, Fishman MC (1993) Targeted disruption of the neuronal nitric oxide synthase gene. Cell 75:1273–1286.

Huang Z, Huang PL, Panahian N, Dalkara T, Fishman MC, Moskowitz MA (1994) Effects of cerebral ischemia in mice deficient in neuronal nitric oxide synthase. Science 265:1883–1885.

Huang Z, Huang PL, Ma J, Meng W, Ayata C, Fishman MC, Moskowitz MA (1996) Enlarged infarcts in endothelial nitric oxide synthase knockout mice are attenuated by nitro-L-arginine. J Cereb Blood Flow Metab 16:981–987.

Inoue S, Kawanishi S (1995) Oxidative DNA damage induced by simultaneous generation of nitric oxide and superoxide. FEBS Lett 371:86–88.

Kamii H, Mikawa S, Murakami K, Kinouchi H, Yoshimoto T, Reola L, Carlson E, Epstein CJ, Chan PH (1996) Effects of nitric oxide synthase inhibition on brain infarction in SOD-1-transgenic mice following

transient focal cerebral ischemia. J Cereb Blood Flow Metab 16:1153–1157.
Lafon-Cazal M, Pietri S, Culcasi M, Bockaert J (1993) NMDA-dependent superoxide production and neurotoxicity. Nature 364:535–537.
Li Y, Sharov VG, Jiang N, Zaloga C, Sabbah HN, Chopp M (1995a) Ultrastructural and light microscopic evidence of apoptosis after middle cerebral artery occlusion in the rat. Am J Pathol 146:1045–1051.
Li Y, Chopp M, Jiang N, Yao F, Zaloga C (1995b) Temporal profile of *in situ* DNA fragmentation after transient middle cerebral artery occlusion in the rat. J Cereb Blood Flow Metab 15:389–397.
Lin KT, Xue JY, Nomen M, Spur B, Wong PYK (1995) Peroxynitrite-induced apoptosis in HL-60 cells. J Biol Chem 270:16487–16490.
Lipton SA, Choi YB, Pan ZH, Lei SZ, Chen HSV, Sucher NJ, Loscalzo J, Singel DJ, Stamler JS (1993) A redox-based mechanism for the neuroprotective and neurodestructive effects of nitric oxide and related nitroso-compounds. Nature 364:626–632.
Löschmann PA, Eblen F, Wüllner U, Klockgether T (1995) NMDA-mediated toxicity to striatal neurons is not reversed by 7-nitroindazole, an inhibitor of neuronal nitric oxide synthase. J Neural Transm Suppl 46:87–95.
Ma J, Ayata C, Huang PL, Fishman MC, Moskowitz MA (1996) Regional cerebral blood flow response to vibrissal stimulation in mice lacking type I NOS gene expression. Am J Physiol 270:1085–1090.
Messmer UK, Ankarcrona M, Nicotera P, Brüne B (1994) p53 expression in nitric oxide-induced apoptosis. FEBS Lett 355:23–26.
Messmer UK, Brüne B (1996) Nitric oxide-induced apoptosis—p53-dependent and p53-independent signalling pathways. Biochem J 319:299–305.
Morikawa E, Huang Z, Moskowitz MA (1992) L-arginine decreases infarct size caused by middle cerebral arterial occlusion in SHR. Am J Physiol 263:1632–1635.
Moskowitz MA, Dalkara T (1996) Nitric oxide and cerebral ischemia. In: Advances in neurology: cellular and molecular mechanisms of ischemic brain damage (Siesjö BK, Wieloch T, eds), pp 365–369. Philadelphia: Lippincott-Raven.
Nicotera P, Bonfoco E, Brüne B (1995) Mechanisms for nitric oxide-induced cell death—involvement of apoptosis. Adv Neuroimmunol 5:411–420.
Palluy O, Rigaud M (1996) Nitric oxide induces cultured cortical neuron apoptosis. Neurosci Lett 208:1–4.
Panahian N, Yoshida T, Huang PL, Hedley-Whyte ET, Dalkara T, Fishman MC, Moskowitz MA (1996) Attenuated hippocampal damage after global cerebral ischemia in mice mutant in neuronal nitric oxide synthase. Neuroscience 72:343–354.
Pelligrino DA (1993) Saying NO to cerebral ischemia. J Neurosurg Anesthesiol 5:221–231.
Poderoso JJ, Carreras MC, Lisdero C, Biobo N, Schöpfer F, Boveris A (1996) Nitric oxide inhibits electron transfer and increases superoxide radical production in rat heart mitochondria and submitochondrial particles. Arch Biochem Biophys 328:85–92.
Qin ZH, Wang YM, Chase TN (1996) Stimulation of *N*-methyl-D-aspartate receptors induces apoptosis in rat brain. Brain Res 725:166–176.
Radi R, Rodriguez M, Castro L, Telleri R (1994) Inhibition of mitochondrial electron transport by peroxynitrite. Arch Biochem Biophys 308:89–95.
Ratan RR, Murphy TH, Baraban JM (1994) Oxidative stress induces apoptosis in embryonic cortical neurons. J Neurochem 62:376–379.
Salgo MG, Bermudez E, Squadrito GL, Pryor WA (1995) Peroxynitrite causes DNA damage and oxidation of thiols in rat thymocytes. Arch Biochem Biophys 322:500–505.
Schulz JB, Matthews RT, Jenkins BG, Ferrante RJ, Siwek D, Henshaw DR, Cipolloni PB, Mecocci P, Kowall NW, Rosen BR, Beal MF (1995) Blockade of neuronal nitric oxide synthase protects against excitotoxicity in vivo. J Neurosci 15:8419–8429.
Schulz JB, Huang PL, Matthews RT, Passow D, Fishman MC, Beal MF (1996) Striatal malonate lesions are attenuated in neuronal nitric oxide synthase knockout mice. J Neurochem 67:430–433.
Stadler J, Billiar TR, Curran RD, Stuehr DJ, Ochoa JB, Simmons RL (1991) Effect of endogenous and exogenous nitric oxide on mitochondrial respiration of rat hepatocytes. Am J Physiol 260:C910–C916.
Szabo C (1996) DNA strand breakage and activation of poly-ADP ribosyltransferase-a cytotoxic pathway triggered by peroxynitrite. Free Radic Biol Med 21:855–869.
Tamir S, Burney S, Tannenbaum SR (1996) DNA damage by nitric oxide. Chem Res Toxicol 9:821–827.
Tilly JL, Hsueh AJW (1993) Microscale autoradiographic method for the qualitative and quantitative analysis of apoptotic DNA fragmentation. J Cell Physiol 154:519–526.
Trotti D, Rossi D, Gjesdal O, Levy LM, Racagni G, Danbolt NC, Volterra A (1996) Peroxynitrite inhibits glutamate transporter subtypes. J Biol Chem 271:5976–5979.
Troy CM, Derossi D, Prochiantz A, Greene LA, Shelanski M (1996) Downregulation of Cu/Zn superoxide dismutase leads to cell death via the nitric oxide-peroxynitrite pathway. J Neurosci 16:253–261.
van Lookeren-Campagne M, Lucassen PJ, Vermeulen JP, Balazs R (1995) NMDA and kainate induce internucleosomal DNA cleavage associated with both apoptotic and necrotic cell death in the neonatal rat brain. Eur J Neurosci 7:1627–1640.
van Lookeren-Campagne M, Gill R (1996) Ultrastructural morphological changes are not characteristic of apoptotic cell death following focal cerebral ischemia in the rat. Neurosci Lett 213:111–114.
Wink DA, Kasprzak KS, Maragos CM, Elespuru RK, Misra M, Dunams TM, Cebula TA, Koch WH, Andrews AW, Allen JS, Keefer LK (1991) DNA deaminating ability and genotoxicity of nitric oxide and its progenitors. Science 254:1001–1003.
Wolvetang EJ, Johnson KL, Krauer K, Ralph SJ, Linnane AW (1994) Mitochondrial respiratory chain inhibitors induce apoptosis. FEBS Lett 339:40–44.
Yoshida T, Limmroth V, Irikura K, Moskowitz MA (1994) The NOS inhibitor, 7-nitroindazole, decreases focal infarct volume but not the response to topical acetylcholine in pial vessels. J Cereb Blood Flow Metab. 14:924–929.
Zhang J, Dawson VL, Dawson TM, Snyder SH (1994) Nitric oxide activation of poly(ADP-ribose) synthetase in neurotoxicity. Science 263:687–689.